Chinese Physical Society | IOP Publishing
CPB
Chinese Physics B
http://cpb.iphy.ac.cn https://iopscience.iop.org/journal/1674-1056

Exceptional point-induced knot structure transformations in non-Abelian braids

Lin-Sheng Bao(包淋升), Jia-Yun Ning(宁佳运), Ao-Qian Shi(史奥芊), Peng Peng(彭鹏), Zhen-Nan Wang(王瑱男), Chao Peng(彭超), Shuang-Chun Wen(文双春), and Jian-Jun Liu(刘建军)

Citation: Chin. Phys. B, 2026, 35 (**1**): 010203. DOI: 10.1088/1674-1056/ae2265
http://cpb.iphy.ac.cn; http://iopscience.iop.org/cpb

Chin. Phys. B **35**, 010203 (2026)

RAPID COMMUNICATION

Exceptional point-induced knot structure transformations in non-Abelian braids

Lin-Sheng Bao(包淋升)[1], Jia-Yun Ning(宁佳运)[1], Ao-Qian Shi(史奥芊)[1], Peng Peng(彭鹏)[1], Zhen-Nan Wang(王瑱男)[1], Chao Peng(彭超)[2], Shuang-Chun Wen(文双春)[1], and Jian-Jun Liu(刘建军)[1,3,†]

[1] *Key Laboratory for Micro/Nano Optoelectronic Devices of Ministry of Education, School of Physics and Electronics, Hunan University, Changsha* 410082, *China*

[2] *State Key Laboratory of Advanced Optical Communication Systems and Networks, Department of Electronics & Frontiers Science Center for Nano-optoelectronics, Peking University, Beijing* 100871, *China*

[3] *Greater Bay Area Institute for Innovation, Hunan University, Guangzhou* 511300, *China*

(Received 16 October 2025; revised manuscript received 19 November 2025; accepted manuscript online 21 November 2025)

The strong connection between braids and knots provides valuable insights into studying the topological state and phase classification of various physical systems. The phenomenon of non-Hermitian (NH) two- and three-band braiding has received widespread attention. However, a systematic exploration and visualization of non-Abelian braiding and the associated knot transformations in four-band systems remains unexplored. Here, we propose a theoretical model of NH four-band braiding, provide its phase diagram, and establish its trivial, Abelian, and non-Abelian braiding rules. Additionally, we report on special knots, such as the Hopf and Solomon links in braided knots, and reveal that their transformations are accompanied by and mediated through exceptional points. Our work provides a detailed case for studying NH multi-band braiding and knot structures in four-band systems, which could offer insights for topological photonics and analog information processing applications.

Keywords: exceptional point, knot structures, phase transitions, non-Abelian braids

PACS: 02.20.–a, 03.65.Vf, 68.35.Rh

DOI: 10.1088/1674-1056/ae2265 **CSTR:** 32038.14.CPB.ae2265

1. Introduction

Recently, braiding has played a prominent role in the fields of condensed matter physics,[1–6] topological quantum,[7–11] and machine learning.[12–14] Braiding is a branch of topology and an important tool for characterizing non-Hermitian (NH) band topology.[15–18] The development of NH band theories has significantly broadened and deepened the understanding of traditional Hermitian bands.[19–24] Unlike Hermitian systems, NH bands exhibit abundant winding and braiding topologies in the complex energy–momentum (E–k) space and can be represented by the braid group B_N. When $N = 2$, B_N is an Abelian group, whereas when $N \geq 3$, B_N is a non-Abelian group.[5,15,25–27] Braids and knots are inextricably linked, and knots can be formed by twisting the strings and joining their ends together.[27–29] Knots have rich structures, including unlinks,[12,13] unknots,[15,18] Hopf links,[28–30] and Solomon links.[31,32] It is impossible for different knots to transform into each other through direct continuous deformation unless they experience a transition state featuring one or multiple touch points.[18,33] In NH systems, braiding phenomena and knot structures are characterized by complex eigenvalues and non-orthogonal eigenvectors, which exhibit complex winding evolution phenomena.[34–37] Specifically, the braiding phenomenon is directly related to the encirclement of exceptional points (EPs), where different knot structures can transform into each other through these EPs.[28,29,38,39]

In NH systems, it has been found both theoretically and experimentally[15,18,34,40,41] that single and double bands can generate complex-energy windings, and double bands exhibit rich braiding structures that can be represented by the braid group B_2. However, the braid group B_2 is merely a simple Abelian group. The most attractive feature of topological braid groups is the non-Abelian characteristic of higher-order braid groups B_N ($N \geq 3$).[12,27,42,43] For NH multiband braiding, non-commutative braiding and non-trivial eigenvalue permutations greatly enrich the study of NH band braiding.[5,26,44] Currently, NH three-band braiding and higher-order braid group B_3 have been partially studied theoretically and experimentally,[16,27,45] but the study of NH multiband braiding phenomena is still in its infancy. Braiding and knots are inseparable, and NH multiband braiding, while inducing rich braiding phenomena, also increases the complexity and difficulty of distinguishing the various structures of knots. While the general classification of 1D non-Hermitian band braiding by the group B_N is well-established,[26–30] a sys-

†Corresponding author. E-mail: jianjun.liu@hnu.edu.cn

http://iopscience.iop.org/cpb http://cpb.iphy.ac.cn

tematic exploration and visualization of non-Abelian braiding and the associated knot transformations in four-band systems remains unexplored. Prior works have pioneered the study of 2-band and 3-band braiding.[28,44] Our work extends this frontier to the four-band case, providing a concrete and comprehensive platform that not only catalogues the achievable braiding phases but also visually bridges the abstract braid group theory, the physical parameter space, and the resulting knot structure transformations.

In this paper, we propose a one-dimensional (1D) tight-binding model to achieve NH four-band braiding, provide its phase diagram controlled by hopping, and establish its trivial, Abelian, and non-Abelian braiding rules, which can be represented by the braid group B_4. By studying the knot structures corresponding to the phase diagram, we discover special knots, such as the Hopf link and Solomon links, and reveal the intrinsic connection between the braiding degrees of the phase diagram and the knots. Furthermore, by studying the continuous phase transitions in the phase diagram, we find evidence for the occurrence of transformations between different knots induced by EPs.

2. Model and theory

In NH multiband systems with nonreciprocal hopping, the NH bands experience topological braiding induced by nonreciprocal hopping as well as phase transitions when they cross boundary lines. Based on previous theoretical studies on NH band braiding and knot structures,[27,45,46] we propose a 1D NH tight-binding model that can be used to study NH four-band braiding. Taking $m = 1$ and $n = 2$ as an example, we illustrate the phase diagram of this NH four-band braid in Fig. 1.

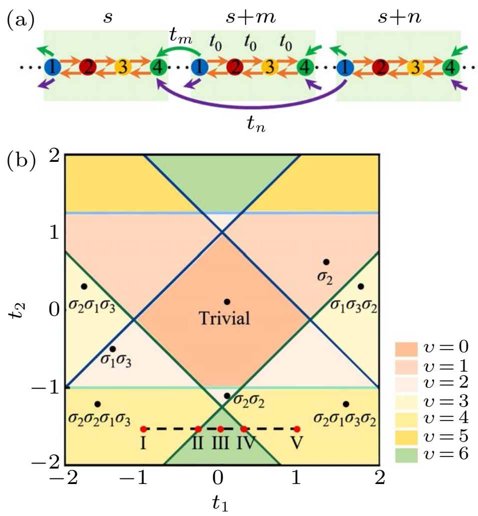

Fig. 1. A 1D NH tight-binding model and an example of its phase diagram. (a) 1D NH tight-binding model. s represents the lattice position, t_m, $t_n \in \mathbb{R}$; $n > m > 0$. (b) Phase diagram for $m = 1$ and $n = 2$. The areas of different colors represent different braiding degrees, and the solid lines of different colors denote the boundary lines.

The 1D NH tight-binding model shown in Fig. 1(a) consists of a unit cell that includes four atomic sites (with zero on-site energy). The neighboring atomic sites are coupled by the reciprocal intracell hopping t_0, and the two nonreciprocal intercell hoppings t_m and t_n represent the long-range hoppings that span m and n unit cells, respectively. The Hamiltonian can be expressed as

$$H(k) = \begin{pmatrix} 0 & t_0 & 0 & 0 \\ t_0 & 0 & t_0 & 0 \\ 0 & t_0 & 0 & t_0 \\ t_m\,\mathrm{e}^{\mathrm{i}mk} + t_n\,\mathrm{e}^{\mathrm{i}nk} & 0 & t_0 & 0 \end{pmatrix}. \tag{1}$$

To study NH four-band braiding, we introduce an integer topological invariant υ to represent the braiding degree of the NH bands,[15,18] which is expressed as

$$\upsilon := \sum_{i,j=1}^{4} \frac{1}{2\pi\mathrm{i}} \oint_{\mathrm{BZ}} \frac{\mathrm{d}\ln \tilde{E}_{i,j}}{\mathrm{d}k}\,\mathrm{d}k, \tag{2}$$

where $\tilde{E}_{i,j} = [E_i(k) - E_j(k)]/2 \ \ (i \neq j)$.

Therefore, we can classify different braiding types according to the braiding degrees and encapsulate them in a phase diagram controlled by intracell and intercell hoppings. For convenience, we set $t_0 = 1$ so that the phase diagram is completely controlled by the intercell hoppings t_m and t_n. Our work focuses on showing the phase diagram and the corresponding band braiding for $m = 1$ and $n = 2$, as shown in Fig. 1(b) (see Section A of the supplementary material[47] for the details of its derivation). According to the phase diagram in Fig. 1(b), we can achieve NH band braiding with a specific braiding degree by selecting appropriate values of t_m and t_n. It should be noted that during the braiding process, the momentum k must evolve over a complete period, i.e., $k \in [k_0, k_0 + 2\pi]$. The braiding process depends on the initial momentum k_0. Considering the positions where the NH bands experience swapping, in order to better present the braiding characteristics of the bands in complex E–k space, we assume $k_0 = \pi/4$ in this work.

3. Results and discussion

3.1. NH four-band braiding

Firstly, the NH four-band braid belongs to the fundamental braid group B_4 (see Section B of the supplementary material[47] for the details of the definition and characteristics of the braid group B_4). We can represent the braiding relations mentioned in this work using a combination of the basic elements σ_1, σ_2, and σ_3 in the braid group B_4. Next, based on the phase diagram shown in Fig. 1(b), we introduce the NH band braiding phenomenon corresponding to different braiding degrees and summarize its braiding characteristics, as shown in Fig. 2.

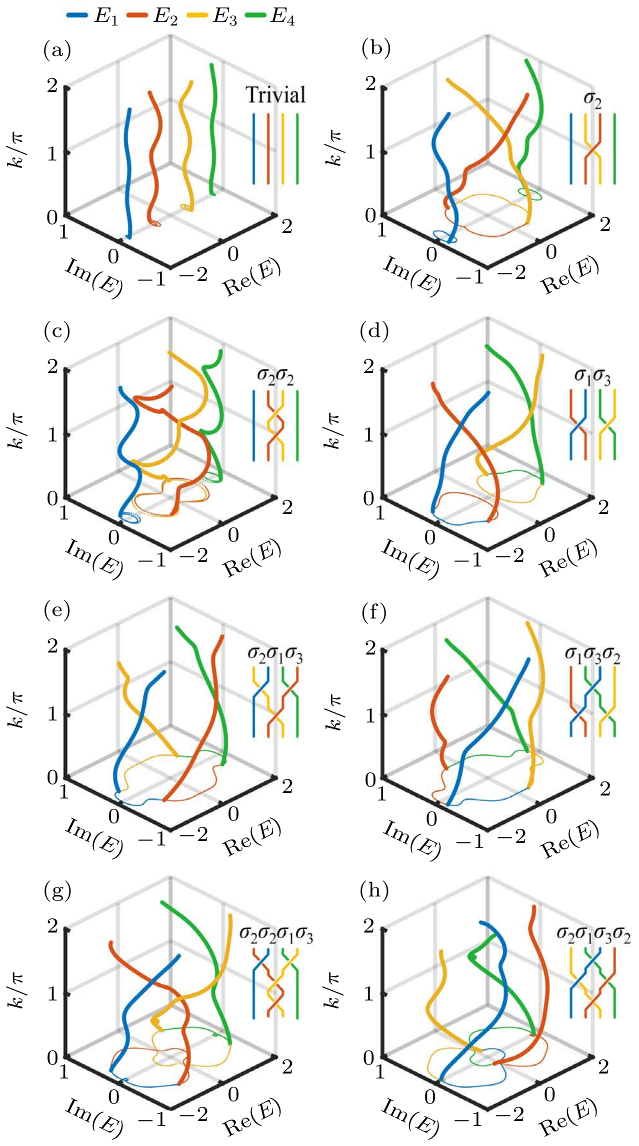

Fig. 2. NH four-band braids corresponding to different braiding degrees for $m = 1$ and $n = 2$. (a) $\upsilon = 0$ ($t_1 = 0.1$ and $t_2 = 0.2$), braid: trivial. (b) $\upsilon = 1$ ($t_1 = 1.3$ and $t_2 = 0.6$), braid: σ_2. (c) $\upsilon = 2$ ($t_1 = 0.1$ and $t_2 = -1.1$), braid: $\sigma_2\sigma_2$. (d) $\upsilon = 2$ ($t_1 = -1.4$ and $t_2 = -0.5$), braid: $\sigma_1\sigma_3$. (e) $\upsilon = 3$ ($t_1 = -1.8$ and $t_2 = 0.3$), braid: $\sigma_2\sigma_1\sigma_3$. (f) $\upsilon = 3$ ($t_1 = 1.8$ and $t_2 = 0.3$), braid: $\sigma_1\sigma_3\sigma_2$. (g) $\upsilon = 4$ ($t_1 = -1.5$ and $t_2 = -1.2$), braid: $\sigma_2\sigma_2\sigma_1\sigma_3$. (h) $\upsilon = 4$ ($t_1 = 1.5$ and $t_2 = -1.2$), braid: $\sigma_2\sigma_1\sigma_3\sigma_2$. In the Re($E$)–Im($E$) plane, the solid lines of different colors represent the projections of the four bands E_1, E_2, E_3, and E_4 evolving from $k = 0$ to $k = 2\pi$. The inset is a schematic of the four-band braid, which is marked in the phase diagram of Fig. 1(b).

Similarly, when $\upsilon = 2$, the four bands are braided twice, but there are two different types of braiding processes (related to the phase diagram in Fig. 1(b)). (1) The bands E_2 and E_3 are braided twice, resulting in [E_1, E_2, E_3, E_4] $\to$ [E_1, E_2, E_3, E_4], with the corresponding braid being represented by $\sigma_2\sigma_2$, as shown in Fig. 2(c). (2) The pairs of bands E_1/E_2 and E_3/E_4 are braided once each, resulting in [E_1, E_2, E_3, E_4] $\to$ [E_2, E_1, E_4, E_3], with the corresponding braid being represented by $\sigma_1\sigma_3$, as shown in Fig. 2(d). Although the three types of braiding processes in Figs. 2(b)–2(d) yield different results, essentially, they can be regarded as simple Abelian braiding processes involving only two bands. After two continuous identical braiding processes, the eigenvalue permutation returns to the initial state. However, non-Abelian braiding occurs when the number of bands involved in the braiding exceeds two. For example, when $\upsilon = 3$, the four bands are braided three times. Like for the case with $\upsilon = 2$, also in this case there are two different types of braiding processes, as illustrated in Figs. 2(e) and 2(f). Unlike for the two types of braiding processes for the case with $\upsilon = 2$, which have different braid group elements, both types of braiding processes for the case with $\upsilon = 3$ are represented by the same braid group elements σ_1, σ_2, and σ_3, with the braids being $\sigma_2\sigma_1\sigma_3$ and $\sigma_1\sigma_3\sigma_2$ in Figs. 2(e) and 2(f), respectively. Similarly, when $\upsilon = 4$, the increase in braiding degree merely results in the addition of another braid group element, namely, σ_2, which still exhibits non-Abelian braiding characteristics, as shown in Figs. 2(g) and 2(h). Therefore, different braid orders result in different eigenvalue permutations, ultimately giving rise to non-Abelian braids. Importantly, the above discussion sheds light on the relationship between braiding degree and braid group. Specifically, the braiding degree matches the number of braid group elements, e.g., for $\upsilon = 3$, there are three corresponding braid group elements, namely, σ_2, σ_1, and σ_3, as shown in Fig. 2(e).

In the same phase diagram, the two different types of braiding processes corresponding to the same braiding degree are related to the distribution of EPs in the NH four-band eigenenergy spectrum. In other words, NH four-band braiding is directly related to the evolution paths of the four bands encircling the EPs. Next, we discuss braiding and nontrivial eigenvalue swapping by studying the encirclement of EPs on Riemann surfaces.[48,49] We replace the k-space Hamiltonian $H(k)$ in Eq. (1) with a parameter-space Hamiltonian $H(\cos(k),\sin(k))$ governed by $\cos(k)$ and $\sin(k)$.[15,50] After transformation, the momentum k can be mapped to a unit circle described by $(\cos(k),\sin(k))$, i.e., $\cos(k)^2+\sin(k)^2 = 1$. Now, we select four cases from Fig. 2 with $\upsilon = 0$ (Fig. 2(a)), $\upsilon = 2$ (Fig. 2(c)), $\upsilon = 3$ (Fig. 2(e)), and $\upsilon = 4$ (Fig. 2(g)) to illustrate the evolution of the eigenvalues on the Riemann surface corresponding to different braiding phenomena, as shown in Fig. 3.

The parameter-space Hamiltonian $H(\cos(k),\sin(k))$ defines the four planes that constitute the Riemann surface shown in Fig. 3. The eigenvalues evolve along different paths on the Riemann surface as the momentum k changes, and their projection onto the $\cos(k)$–$\sin(k)$ plane clearly shows the eigenvalue evolution paths crossing the EPs and their branch cuts. Note that due to the distribution of EPs in complex E–k space, there are cases where the projections of two EPs overlap in this plane: In Figs. 3(b) and 3(d), the red dot 1 and red line 1 represent the projections of EP_1 and EP_5, along with their branch cuts, and the red dot 3 and red line 3 represent the projections of EP_2 and EP_6, along with their branch cuts. In Fig. 3(c), the red dot 2 and red line 2 represent the projections of EP_1 and EP_3, along with their branch cuts. Different braiding degrees correspond to different evolution paths of the bands encircling the EPs, leading to different eigenvalue permutations.[36,37] In Fig. 3(a), the eigenvalues are not swapped since the evolution paths do not cross the EPs, which corresponds to the independent and trivial evolution of the four bands illustrated in Fig. 2(a) for $\upsilon = 0$. By contrast, when the evolution paths of the bands encircle the EPs, it is inevitable that the branch cuts cross on the Riemann surface, which leads to the eigenvalues being swapped. As shown in Fig. 3(b), the evolution paths of the bands sequentially cross the branch cut red lines 4 and 2, encircling two EPs (EP_3 and EP_4). The eigenvalues change from $[E_1, E_2, E_3, E_4]$ to $[E_1, E_3, E_2, E_4]$ and then back to $[E_1, E_2, E_3, E_4]$, which corresponds to the braid $\sigma_2\sigma_2$ displayed in Fig. 2(c). Similarly, in Figs. 3(c) and 3(d), the evolution paths of the bands encircle three EPs (EP_1, EP_2, and EP_3) and four EPs (EP_3, EP_4, EP_2, and EP_6) in sequence, resulting in three and four braids, respectively. These braids correspond to Figs. 2(e) and 2(g), respectively. Thus, NH band braiding is closely related to the evolution paths of the bands encircling the EPs, and the number of EPs encircled determines the value of the braiding degree υ.

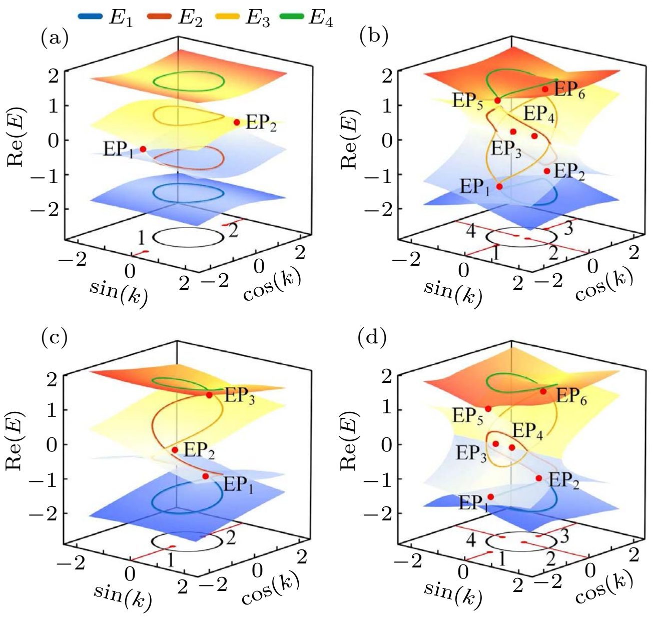

Fig. 3. Evolution of the eigenvalues on Riemann surfaces for different braiding degrees. (a) $\upsilon = 0$ ($t_1 = 0.1$ and $t_2 = 0.2$). (b) $\upsilon = 2$ ($t_1 = 0.1$ and $t_2 = -1.1$). (c) $\upsilon = 3$ ($t_1 = -1.8$ and $t_2 = 0.3$). (d) $\upsilon = 4$ ($t_1 = -1.5$ and $t_2 = -1.2$). The solid lines of different colors on the Riemann surface represent the eigenvalue evolution paths, and the red dots represent the EPs on the Riemann surface. In the $\cos(k)$–$\sin(k)$ plane, the black circles represent the projection of the eigenvalue evolution path, and the red dots and red lines represent the projections of EPs and their branch cuts, respectively, with numbers indicating them.

3.2. Formation and transformations of knot structures

NH band braiding is accompanied by the emergence of knot structures. The NH band braiding discussed in this work is based on the evolution of the momentum k over one period. However, if the ends of the braided bands are connected, their knot structures can be determined. Taking the braiding example with $\upsilon = 4$ in Fig. 2(g), we demonstrate how the knot structures are generated, and we summarize the transitions corresponding to different braiding degrees shown in the phase diagram of Fig. 1(b), as presented in Fig. 4.

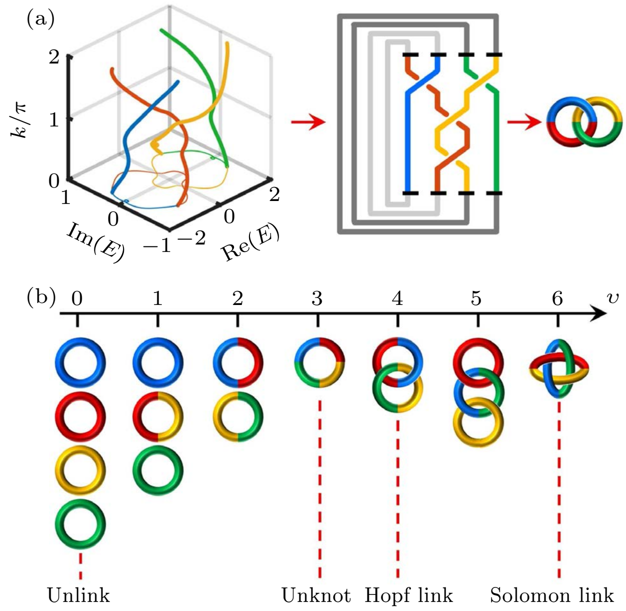

Fig. 4. Example of the formation of knot structures and their correspondence to braiding degree. (a) Formation of the knot structures for $\upsilon = 4$. The solid grey lines in the middle subfigure indicate the connection of the ends of the bands. (b) Different braiding degrees correspond to different knot structures. The red dashed lines indicate several special knots.

In Fig. 4(a), the left subfigure shows NH four-band braiding with $\upsilon = 4$, which is represented by the braid $\sigma_2\sigma_2\sigma_1\sigma_3$. To illustrate the transition from band braiding to a knot, we have added additional auxiliary lines to the diagram of the braid represented by $\sigma_2\sigma_2\sigma_1\sigma_3$, as shown in the middle subfigure of Fig. 4(a). We use two different lines (of different gray colors) to connect the ends of the bands where the evolution finishes, eventually forming a knot. Lines of the same color indicate that a ring can be formed after connection. For example, the light-gray lines connect the ends of the red and blue braiding bands, which thus form a ring; this ring is then combined with the ring formed by the yellow and green braiding bands (connected by the dark-gray lines) to give rise to a Hopf link, as shown in the right subfigure of Fig. 4(a). Thus, in NH multiband systems, by utilizing auxiliary lines, one or multiple bands collectively form a ring, and then the individual rings wind around each other to form a unique knot.[15,28]

Based on the phase diagram with $m = 1$ and $n = 2$ shown in Fig. 1(b), we study the knot structures corresponding to each braiding degree, as shown in Fig. 4(b). When $\upsilon = 0$, due to the trivial braiding, the four bands evolve independently, and the resulting knots are four separate rings, known as unlinks.

However, with increasing braiding degree, the obtained knot constantly changes. From $\upsilon = 0$ to $\upsilon = 6$, the braided knot transforms from the initial four separate rings, which are unlinks, through continuous evolution, to a final complex knot structure, known as the Solomon link. Simultaneously, during this process, other knots appear, such as an unknot for $\upsilon = 3$, and a Hopf link for $\upsilon = 4$. For a given phase diagram, the knot structures obtained through band braiding can vary continuously with the braiding degree, enabling continuous transitions between different knots.

Next, we clarify the nature of transformations between different knot structures for a given phase diagram. We select five representative cases on the black dashed line in the phase diagram of Fig. 1(b) to analyze and explain the transformations between the knot structures, as shown in Fig. 5.

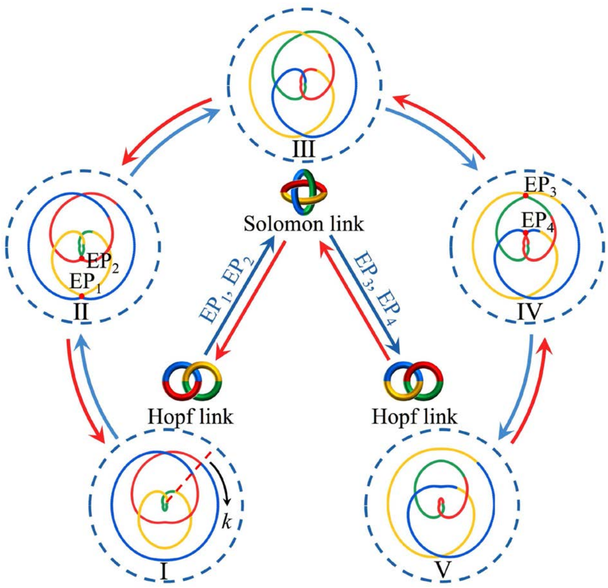

Fig. 5. Knot structure transformations and transition states. The four solid lines inside the blue dashed circle indicate the evolution of the four bands with momentum k in polar coordinates. The red dashed line indicates the starting point of the evolution of the momentum k. The evolution proceeds in the direction of the black arrow. Stages ① ($t_1 = -1.0$ and $t_2 = -1.5$) and ⑤ ($t_1 = 1.0$ and $t_2 = -1.5$) result in a Hopf link, stage ③ ($t_1 = 0$ and $t_2 = -1.5$) corresponds to a Solomon link, and stages ② ($t_1 = -0.25$ and $t_2 = -1.5$) and ④ ($t_1 = 0.25$ and $t_2 = -1.5$) represent the transition states between stage ① and stage ③, and between stage ③ and stage ⑤, respectively, Both these transition states contain two EPs. Stages ① and ⑤ experience continuous phase transitions along the peripheral blue (red) arrows in a clockwise (counterclockwise) direction.

We change the evolution of momentum k and transform the band from the complex E–k space braiding to a two-dimensional (2D) knot structure (see Section D of the supplementary material[47] for the details of the complex E–k space braiding). The NH four-band braiding in stages ①, ③, and ⑤ in Fig. 5 corresponds to a Hopf link, Solomon link, and Hopf link, respectively, which is consistent with the knot structures obtained for $\upsilon = 4$ and $\upsilon = 6$ in Fig. 4. Next, we analyze the knot structure transformation in the transition state, taking the transformation from stage ① (Hopf link) to stage ③ (Solomon link) as an example (indicated by the blue arrow in Fig. 5). From the phase diagram in Fig. 1(b), we can observe that during the transition from stage ① to stage ③, the nonreciprocal hopping t_2 remains constant, while t_1 changes continuously and crosses the boundary line where stage ② is located. In Fig. 5, stage ② serves as a transition state from stage ① to stage ③, featuring two degenerate points, namely, EP_1 and EP_2. Therefore, the essence of the transformation from stage ① to stage ③ is the braided phase transition of NH bands when the nonreciprocal hopping t_1 crosses EPs. Similarly, there are two degenerate points in stage ④, namely, EP_3 and EP_4. The phase transition in this case also occurs when the nonreciprocal hopping t_1 crosses these two EPs. The nonreciprocal hopping t_1 in stages ② and ④ crosses different EPs, resulting in different ways in which the bands in stages ① and ⑤ can be connected, although both result in the formation of Hopf links. Although stages ② and ④ in Fig. 5 do not give rise to any special knot, they are key evidence demonstrating the transformations of the knot structures. Not only can this prove that the value of υ is related to the number of times the EPs are encircled (consistent with the conclusion in Fig. 3), but it can also indicate that the boundary lines of the phase diagram are composed of different numbers of EPs (consistent with the conclusion in Section A of the supplementary material[47]). Additionally, if we change the transformation direction in Fig. 5 so that stage ⑤ continuously evolves to stage ① (along the direction of the red arrow), the above conclusions are still valid because the encircling EPs are the same. Therefore, our work provides evidence that transformations between different knot structures are induced by EPs.

4. Conclusion

In summary, we presented a systematic investigation of NH four-band braiding, provided its phase diagram, and established its trivial, Abelian, and non-Abelian braiding rules, which can be represented by the braid group B_4. Additionally, we discovered special knots, such as the Hopf and Solomon links, by showing the knot structures corresponding to different braids and unveiled that the transitions between these distinct knot structures occur at parameter boundaries defined by exceptional points. Our results provide a concrete and visualizable platform for the study of NH multiband braiding and the non-Abelian characteristics of higher-order braid groups. The controllable manipulation of topological knots via system parameters may inspire novel approaches in topological photonic devices and classical information processing schemes based on topological invariants. For instance, in topological photonics, such EP-driven knot transformations could be leveraged to design reconfigurable optical devices[51] or switching schemes[52] where the knot type serves as a robust topological state variable. Furthermore, the principles of our 1D tight-binding model are not limited to four bands. The approach can be generalized to systems with $N > 4$ bands, where the braid group B_N exhibits even richer non-Abelian structures. Exploring these higher-band systems could uncover more complex knots and braiding phenomena, offering a fertile ground for future theoretical and experimental work in topological metamaterials.

The proposed 1D NH tight-binding model is amenable to experimental implementation in several advanced platforms. For example, photonic waveguide arrays[53] offer precise control over hopping amplitudes and engineered losses, providing an ideal setting to map our Hamiltonian and directly observe the complex energy braids and their associated knot structures. Similarly, synthetic dimension lattices implemented in photonic systems or with ultracold atoms[15,16,54] can emulate the multi-band tight-binding dynamics and probe the requisite momentum-space topology. Additionally, acoustic or electrical circuit networks have emerged as versatile and highly controllable testbeds for non-Hermitian physics[18,27–29,36,55] and could be tailored to realize the non-reciprocal hopping terms and detect the knot structure transformations predicted in our work.

Acknowledgements

This work was supported by the National Natural Science Foundation of China (Grant Nos. 62575099, 62075059, and 61405058), Guangdong Basic and Applied Basic Research Foundation (Grant No. 2024A1515011353), Open Project of the State Key Laboratory of Advanced Optical Communication Systems and Networks of China (Grant No. 2024GZKF20), the Natural Science Foundation of Hunan Province (Grant Nos. 2020JJ4161 and 2017JJ2048), and Scientific Research Foundation of Hunan Provincial Education Department (Grant No. 21A0013).

References

[1] Yang Y, Yang B, Ma G, Li J, Zhang S and Chan C T 2024 *Science* **383** eadf9621
[2] Slager R J, Bouhon A and Ünal F N 2024 *Nat. Commun.* **15** 1144
[3] Pang Z, Wong B T T, Hu J and Yang Y 2024 *Phys. Rev. Lett.* **132** 043804
[4] Sun X C, Wang J B, He C and Chen Y F 2024 *Phys. Rev. Lett.* **132** 216602
[5] Long Y, Wang Z, Zhang C, Xue H, Zhao Y X and Zhang B 2024 *Phys. Rev. Lett.* **132** 236401
[6] Shan Z L, Sun Y K, Tao R, Chen Q D, Tian Z N and Zhang X L 2024 *Phys. Rev. Lett.* **133** 053802
[7] Nayak C, Simon S H, Stern A, Freedman M and Das Sarma S 2008 *Rev. Mod. Phys.* **80** 1083
[8] Iqbal M, Tantivasadakarn N, Verresen R and Vishwanath A 2023 *Phys. Rev. Lett.* **131** 060405
[9] Campbell S L, Dreiling J M, Figgatt C, Gaebler J P, Johansen J, Mills M, Moses S A, Pino J M, Ransford A, Rowe M, Siegfried P, Stutz R P, Foss-Feig M, Vishwanath A and Dreyer H 2024 *Nature* **626** 501
[10] Tsintzis A, Souto R S, Flensberg K, Danon J and Leijnse M 2024 *PRX Quantum* **5** 010323
[11] Petiziol F 2024 *Phys. Rev. Lett.* **133** 036601
[12] Long Y, Xue H and Zhang B 2024 *Nat. Mach. Intell.* **6** 904
[13] Chen J, Wang Z, Tan Y T, Wang C and Ren J 2024 *Commun. Phys.* **7** 209
[14] Gukov S, Halverson J and Ruehle F 2024 *Nat. Rev. Phys.* **6** 310
[15] Wang K, Dutt A, Wojcik C C and Fan S 2021 *Nature* **598** 59
[16] Patil Y S S, Höller J, Henry P A, Guria C, Zhang Y, Jiang L, Kralj N, Read N and Harris J G E 2022 *Nature* **607** 271
[17] Guo C X, Chen S, Ding K and Hu H 2023 *Phys. Rev. Lett.* **130** 157201
[18] Zhang Q, Li Y, Sun H, Liu X, Zhao L, Feng X, Fan X and Qiu C 2023 *Phys. Rev. Lett.* **130** 017201
[19] Okuma N, Kawabata K, Shiozaki K and Sato M 2020 *Phys. Rev. Lett.* **124** 086801
[20] Zhu W and Gong J 2023 *Phys. Rev. B* **108** 035406
[21] Li Z, Wang L W, Wang X, Lin Z K, Ma G and Jiang J H 2024 *Nat. Commun.* **15** 6544
[22] Chen J, Shi A, Peng Y, Peng P and Liu J 2024 *Chin. Phys. Lett.* **41** 037103
[23] Shi A, Bao L, Peng P, Ning J, Wang Z and Liu J 2025 *Phys. Rev. B* **111** 094109
[24] Peng Y, Shi A, Peng P and Liu J 2025 *Phys. Rev. B* **111** 085148
[25] Wojcik C C, Sun X Q, Bzdušek T and Fan S 2020 *Phys. Rev. B* **101** 205417
[26] Li Z and Mong R S K 2021 *Phys. Rev. B* **103** 155129
[27] Zhang Q, Zhao L, Liu X, Feng X, Xiong L, Wu W and Qiu C 2023 *Phys. Rev. Res.* **5** L022050
[28] Hu H and Zhao E 2021 *Phys. Rev. Lett.* **126** 010401
[29] Li Z, Ding K and Ma G 2023 *Phys. Rev. Res.* **5** 023038
[30] Rafi-Ul-Islam S M, Siu Z B, Razo M S H, Sahin H and Jalil M B A 2024 *Phys. Rev. B* **110** 045444
[31] Cao W, Zhang W and Zhang X 2024 *Phys. Rev. B* **109** 165128
[32] Zhu B, Wang Q, Wang Y, Wang Q J and Chong Y D 2024 *Phys. Rev. B* **110** 134317
[33] Yang Z, Chiu C K, Fang C and Hu J 2020 *Phys. Rev. Lett.* **124** 186402
[34] Wang K, Dutt A, Yang K Y, Wojcik C C, Vučković J and Fan S 2021 *Science* **371** 1240
[35] Ding K, Fang C and Ma G 2022 *Nat. Rev. Phys.* **4** 745
[36] Tang W, Ding K and Ma G 2022 *Nat. Sci. Rev.* **9** nwac010
[37] Bao L, Shi A, Peng Y, Peng P, Ning J, Wang Z, Peng C and Liu J 2024 *Phys. Rev. B* **110** L020104
[38] Lee C H, Li L, Thomale R and Gong J 2020 *Phys. Rev. B* **102** 085151
[39] Hu H, Sun S and Chen S 2022 *Phys. Rev. Res.* **4** L022064
[40] Shen H, Zhen B and Fu L 2018 *Phys. Rev. Lett.* **120** 146402
[41] Li Y, Ji X, Chen Y, Yan X and Yang X 2022 *Phys. Rev. B* **106** 195425
[42] Zhang X, Yu F, Chen Z, Tian Z, Chen Q D, Sun H B and Ma G 2022 *Nat. Photon.* **16** 390
[43] Chen Z, Zhang R, Chan C T and Ma G 2022 *Nat. Phys.* **18** 179
[44] Zhong Q, Khajavikhan M, Christodoulides D N and El-Ganainy R 2018 *Nat. Commun.* **9** 4808
[45] Midya B 2023 *Appl. Phys. Lett.* **123** 123101
[46] Yao S and Wang Z 2018 *Phys. Rev. Lett.* **121** 086803
[47] See supplementary material for the derivation of phase diagrams for the tight-binding model, the definition and characteristics of the braid group B_4, the NH four-band braiding with $\upsilon = 5$ and $\upsilon = 6$ and the topological phase transitions and transition states of braided knots in complex E–k space
[48] Guria C, Zhong Q, Ozdemir S K, Patil Y S S, El-Ganainy R and Harris J G E 2024 *Nat. Commun.* **15** 1369
[49] Tang Z, Chen T, Tang X and Zhang X 2024 *Light Sci. Appl.* **13** 167
[50] Guo Q, Jiang T, Zhang R Y, Zhang L, Zhang Z Q, Yang B, Zhang S and Chan C T 2021 *Nature* **594** 195
[51] Yan Q C, Zhao B H, Zhou R, Ma R, Lyu Q H, Chu S S, Hu X Y and Gong Q H 2023 *Nanophotonics* **12** 2247
[52] Ke S L, Wang B, Long H, Wang K and Lu P X 2017 *Opt. Quant. Electron.* **49** 224
[53] Zhang B, Yan W and Chen F 2025 *Adv. Photon.* **7** 034002
[54] Yu D, Song W, Wang L, Srikanth R, Sridhar S, Chen T, Huang C, Li G, Qiao X, Wu X, Dong Z, He Y, Xiao M, Chen X, Dutt A, Gadway B and Yuan L 2025 *Photon. Insights* **4** R06
[55] Leykam D, Andreanov A and Flach S 2018 *Adv. Phys. X* **3** 1473052